Science Advances
AAAS

advances.sciencemag.org/cgi/content/full/5/2/eaav2437/DC1

Supplementary Materials for

Targeting DDR2 enhances tumor response to anti–PD-1 immunotherapy

Megan M. Tu, Francis Y. F. Lee, Robert T. Jones, Abigail K. Kimball, Elizabeth Saravia, Robert F. Graziano, Brianne Coleman, Krista Menard, Jun Yan, Erin Michaud, Han Chang, Hany A. Abdel-Hafiz, Andrii I. Rozhok, Jason E. Duex, Neeraj Agarwal, Ana Chauca-Diaz, Linda K. Johnson, Terry L. Ng, John C. Cambier, Eric T. Clambey, James C. Costello, Alan J. Korman, Dan Theodorescu*

*Corresponding author. Email: dan.theodorescu@cshs.org

Published 20 February 2019, *Sci. Adv.* **5**, eaav2437 (2019)
DOI: 10.1126/sciadv.aav2437

The PDF file includes:

Other Supplementary Material for this manuscript includes the following:

(available at advances.sciencemag.org/cgi/content/full/5/2/eaav2437/DC1)

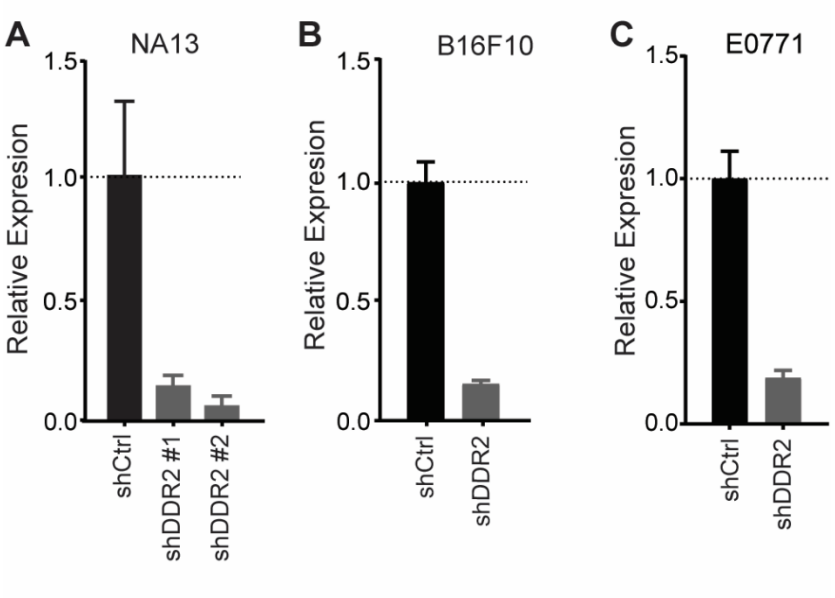

Fig. S1. shRNA-mediated knockdown of DDR2 expression. qPCR analysis of (**A),** NA13 shControl (shCtrl), and shDDR2 #1 and #2. (**B),** B16F10 shCtrl and shDDR2. (**C),** E0771 shCtrl and shDDR2. 18s was used as an internal control for normalization of mRNA levels across different samples.

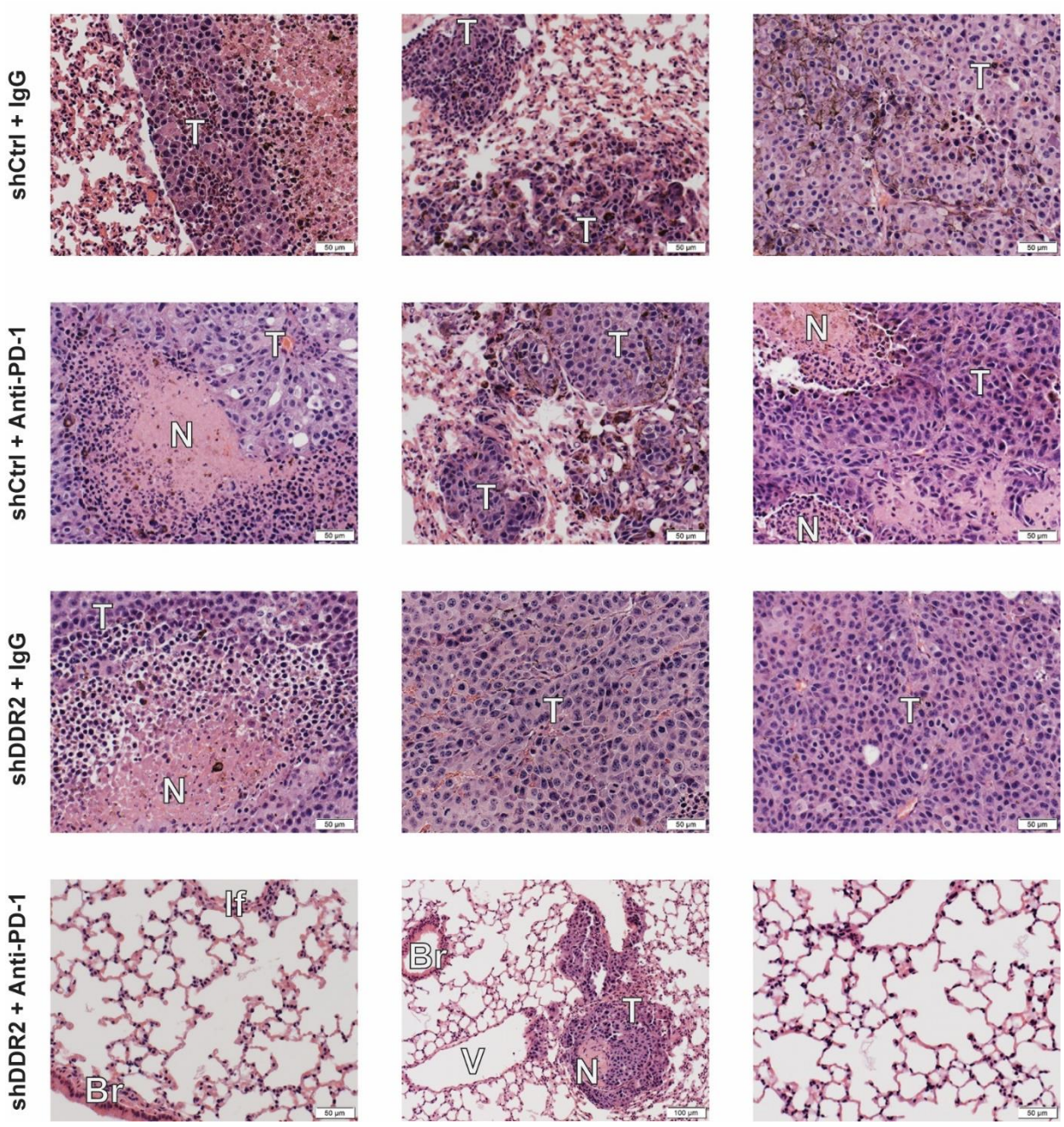

Fig. S2. Histological comparison of lungs from B16F10 tumor–bearing mice. (**A**), Representative H&E images from the lungs of mice injected intravenously with B16F10 to form pulmonary metastases. T, tumor; N, necrosis; If, inflammation; Br, bronchiole; V, vein.

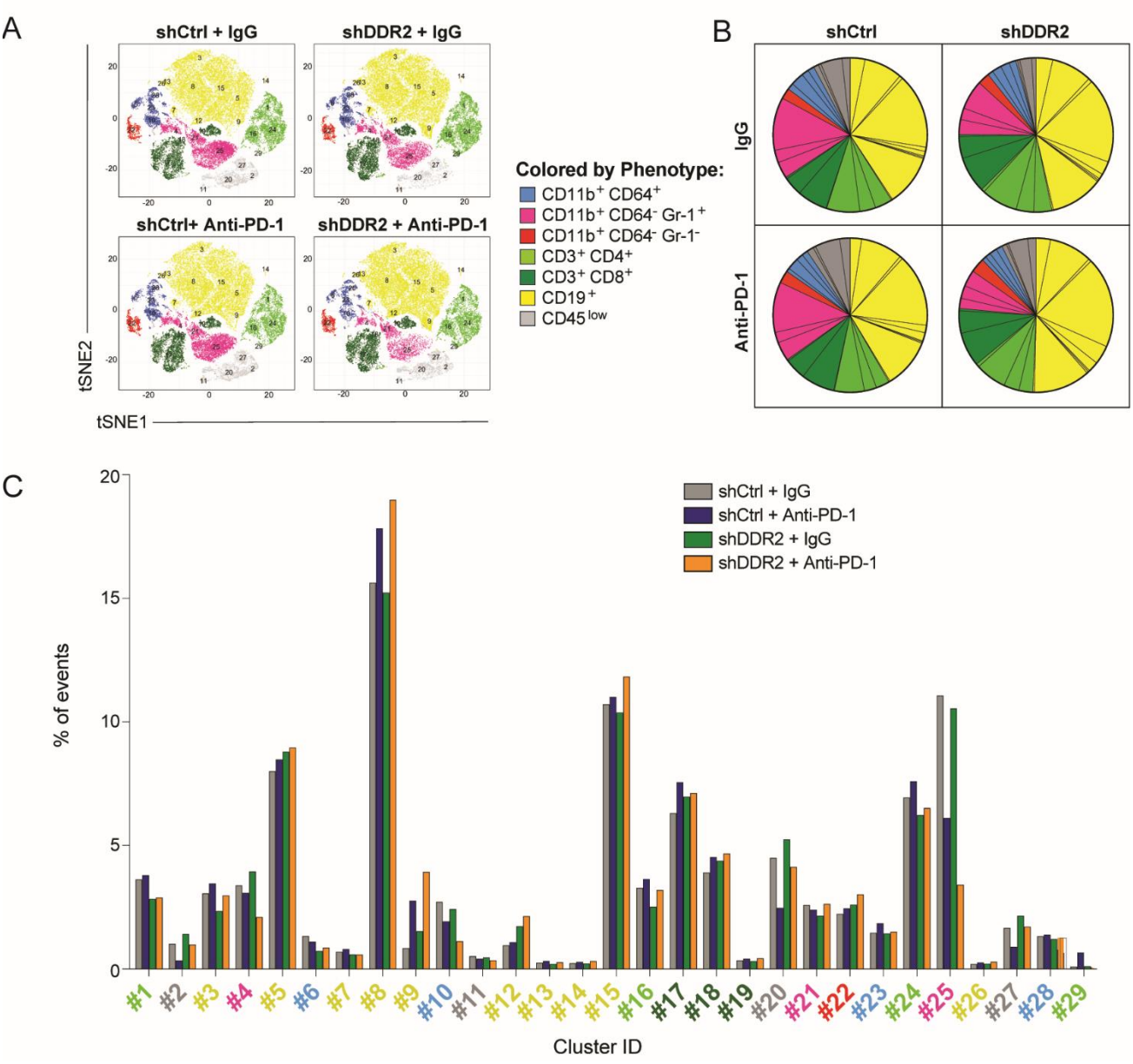

Fig. S3. Spleen from NA13 tumor–bearing mice analyzed using CyTOF with PhenoGraph algorithm. (**A**)**,** PhenoGraph-defined cellular distribution and clustering, as defined by tSNE1 and tSNE2, colored by phenotype designation for each experimental condition (data pooled from *n* =5-6 mice per group). Data shows all normalized viable single cells, subjected to the PhenoGraph algorithm. (**B**)**,** Pie charts show the cellular distribution of 29 PhenoGraph defined clusters colored according to phenotypic designation. **c,** Frequency of events across 29 PhenoGraph defined clusters for each experimental condition. Each colored number represents the phenotype which these clusters fall into.

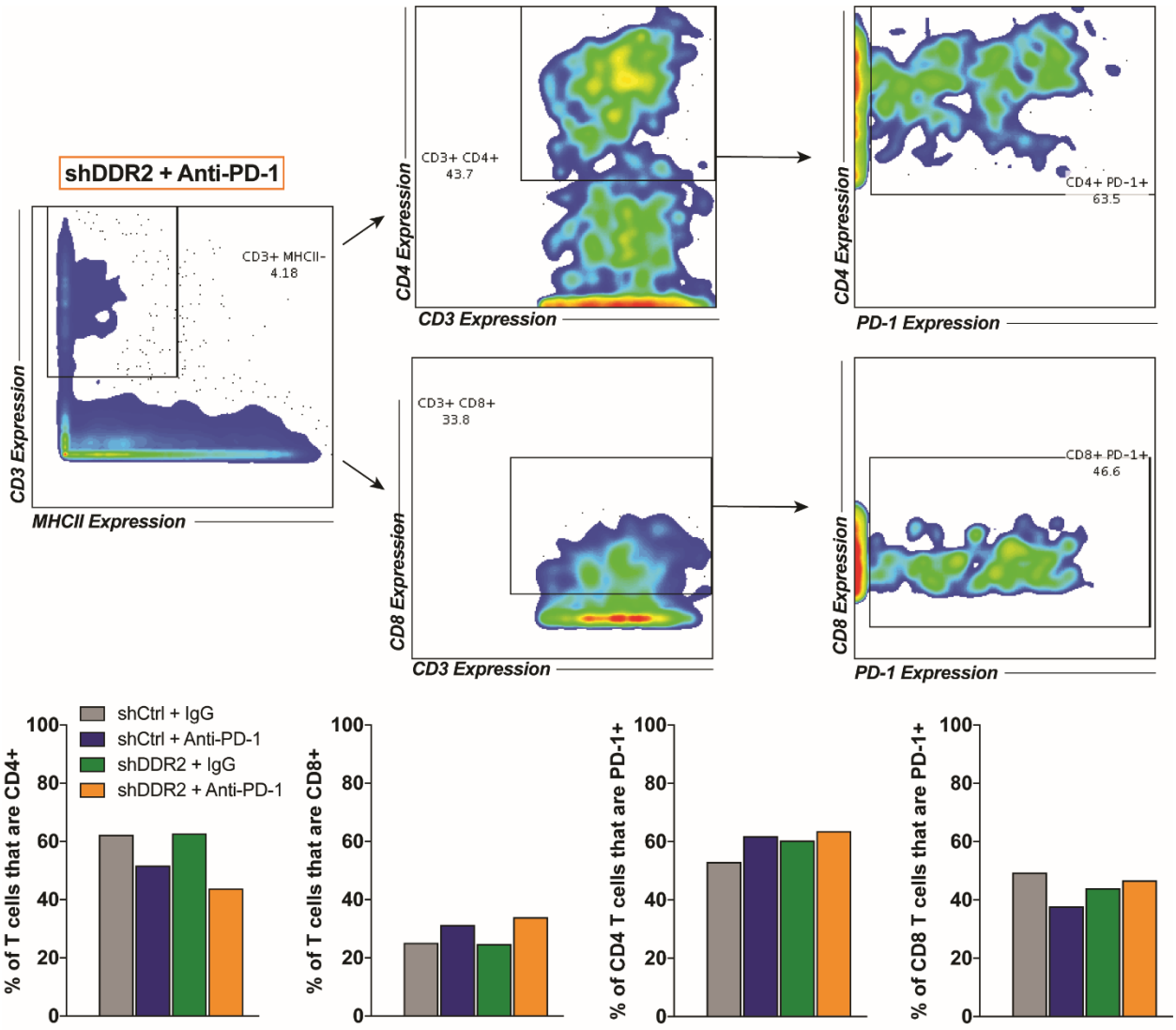

Fig. S4. Analysis of PD-1 expression on tumor-infiltrating T cells. Files that were previously gated for 191^{+} 193^{+} 195^{-} events and concatenated according to group and used for the PhenoGraph analysis found in Fig. 3B are shown. Files were further gated for T cells (defined as: $CD3^{+}$ MHC-II^{-} events), CD4 T cells ($CD3^{+}$ $CD4^{+}$ MHC-II^{-} events), CD8 T cells ($CD3^{+}$ $CD8^{+}$ MHC-II^{-} events), PD-1^{+} CD4 T cells ($CD3^{+}$ $CD4^{+}$ MHC-II^{-} PD-1^{+} events), and PD-1^{+} CD8 T cells ($CD3^{+}$ $CD8^{+}$ MHC-II^{-} PD-1^{+} events).

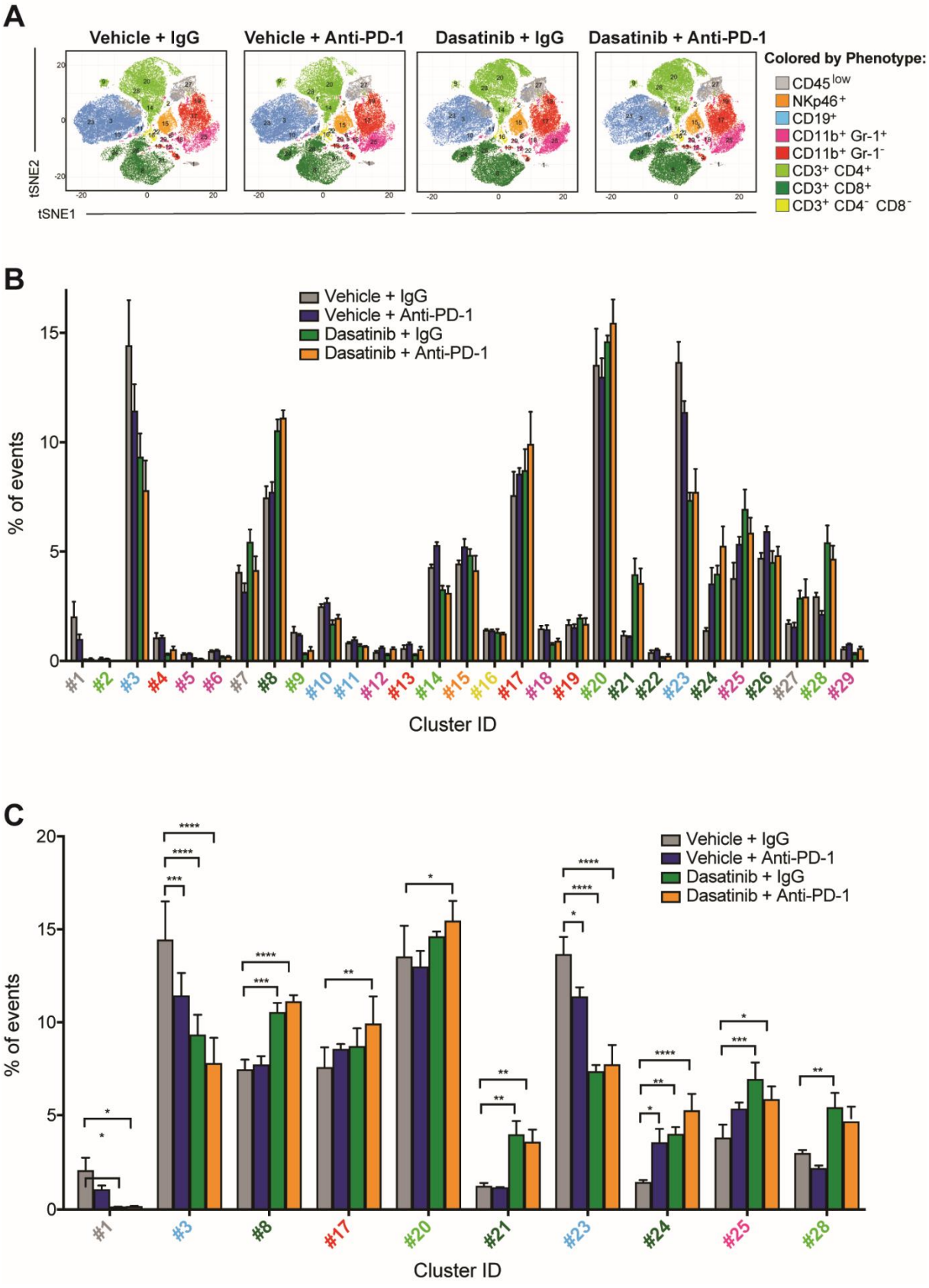
A
Vehicle + IgG
Vehicle + Anti-PD-1
Dasatinib + IgG
Dasatinib + Anti-PD-1
tSNE2
tSNE1
Colored by Phenotype:
CD45 low
NKp46+
CD19+
CD11b+ Gr-1+
CD11b+ Gr-1-
CD3+ CD4+
CD3+ CD8+
CD3+ CD4- CD8-
B
Vehicle + IgG
Vehicle + Anti-PD-1
Dasatinib + IgG
Dasatinib + Anti-PD-1
% of events
Cluster ID
C
Vehicle + IgG
Vehicle + Anti-PD-1
Dasatinib + IgG
Dasatinib + Anti-PD-1
% of events
Cluster ID

Fig. S5. Spleen from MC38 tumor–bearing mice analyzed using CyTOF with PhenoGraph algorithm. (**A**)**,** PhenoGraph-defined cellular distribution and clustering, as defined by tSNE1 and tSNE2, colored by cellular phenotype for all treatment conditions (n = 4 mice per group). Data shows all normalized viable single cells, subjected to the PhenoGraph algorithm. (**B**)**,** Frequency of all 29 PhenoGraph identified clusters, colored according to experimental group and cluster's primary phenotype designation. (**C**)**,** The frequency of all statistically significant PhenoGraph identified clusters compared to Vehicle + IgG organized according to cluster phenotypic designation. *$P < 0.05$, **$P < 0.01$, ***$P < 0.001$, ****$P < 0.0001$.

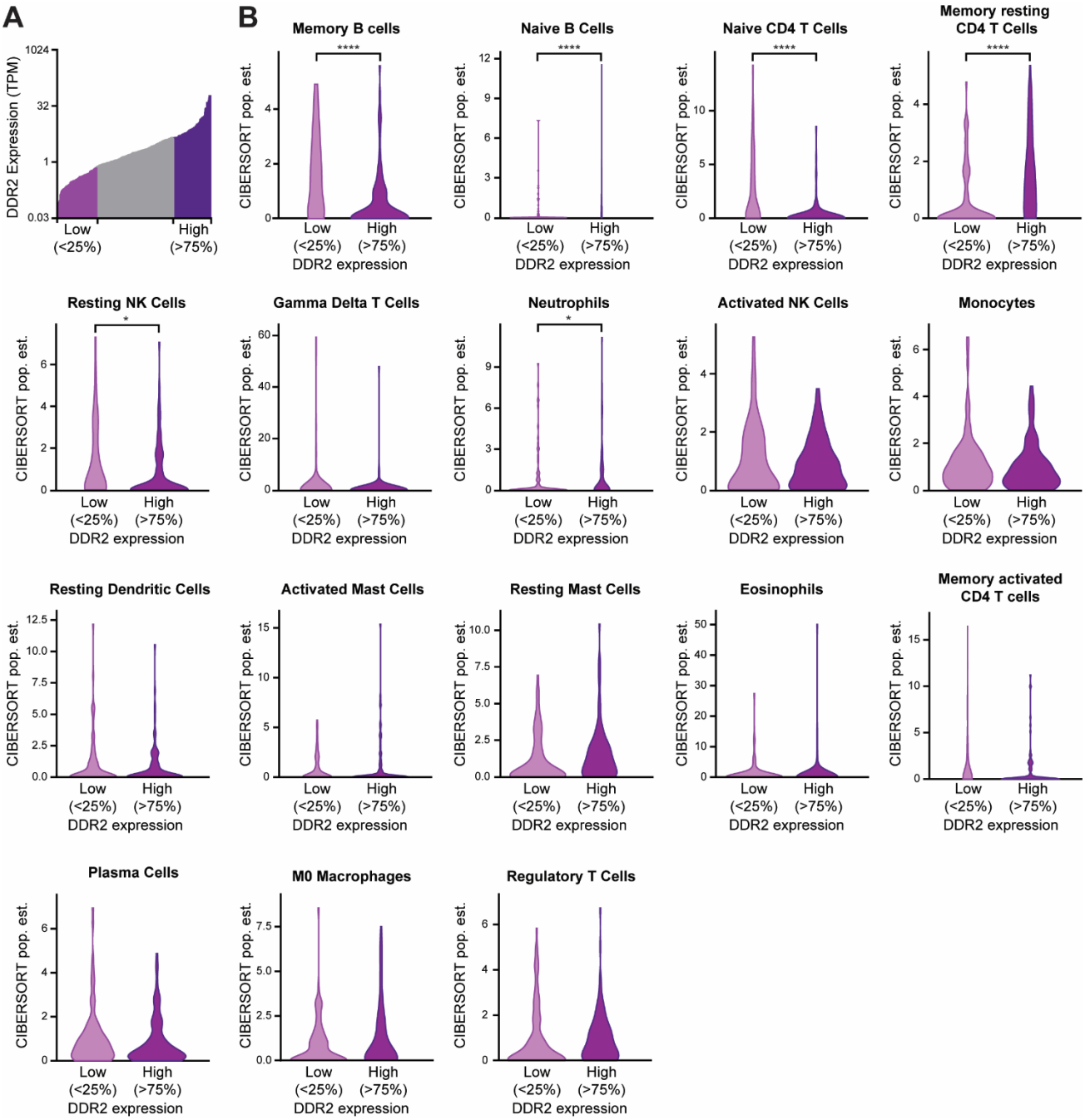

Fig. S6. Quantification of immune cell populations in bladder cancer patients with varying DDR2 expression levels. (**A**)**,** Distribution of DDR2 expression in quartiles. (**B**)**,** Relative abundance of tumor-infiltrating immune cell populations determined by CIBERSORT methodology (*24*) in bladder cancer patients from RNAseq data in the TCGA (n = 433). **P* < 0.05, ***P* < 0.01, ****P* < 0.001, *****P* < 0.0001.

Table S4. CyTOF antibody panel used for the analysis of spleen and tumors from mice implanted with the NA13 cell line.

Target	Clone	Tag	Source
CD45	30-F11	89Y	Fluidigm
Ly-6G/C (Gr-1)	RB6-8C5	141Pr	Fluidigm
CD11c	N418	142Nd	Fluidigm
CD357 (GITR)	DTA1	143Nd	Fluidigm
MHC-I	28-14-8	144Nd	Fluidigm
CD69	H1.2F3	145Nd	Fluidigm
CD8α	53-6.7	146Nd	Fluidigm
CD11b	M1/70	148Nd	Fluidigm
CD19	6D5	149Sm	Fluidigm
CD25	3C7	150Nd	Fluidigm
CD64	X54-5/7.1	151Eu	Fluidigm
CD3ε	145-2C11	152Sm	Fluidigm
CD274 (PD-L1)	10f.9G2	153Eu	Fluidigm
CD152 (CTLA-4)	UC10-4B9	154Sm	Fluidigm
IRF4	3E4	155Gd	Fluidigm
Foxp3	FJK-16s	158Gd	Fluidigm
CD279 (PD-1)	RMP1-30	159Tb	Fluidigm
Tbet	4B10	161Dy	Fluidigm
CD366 (Tim-3)	RMT3-23	162Dy	Fluidigm
Arginase-1	polyclonal	166Er	Fluidigm
NKp46	29A1.4	167Er	Fluidigm
Ki-67	B56	168Er	Fluidigm
CD49b	HMa2	170Er	Fluidigm
CD44	IM7	171Yb	Fluidigm
CD4	RM4-5	172Yb	Fluidigm
CD223/LAG3	C9B7W	174Yb	Fluidigm
CD127	A7R34	175Lu	Fluidigm
CD278/ICOS	7E.17G9	176Yb	Fluidigm
Live/Dead	*N/A*	195Pt	Fluidigm
MHC-II (I-A/I-E)	M5/114.15.2	209Bi	Fluidigm

Table S5. CyTOF antibody panel used for the analysis of tumors from mice implanted with the MC38 cell line.

Target	Clone	Tag	Source
Ly6G/C (Gr-1)	RB6-8C5	141Pr	Fluidigm
CD11c	N418	142^{Nd}	Fluidigm
CD69	H1.2F3	145Nd	Fluidigm
CD45	30-F11	147Sm	Fluidigm
CD11b (MAC1)	M1/70	148Nd	Fluidigm
CD19	6D5	149Sm	Fluidigm
CD25	3C7	151Eu	Fluidigm
CD3e	145-2C11	152Sm	Fluidigm
TER-119	TER119	154Sm	Fluidigm
CD62L	MEL-14	160Gd	Fluidigm
CD8a	53-6.7	168Er	Fluidigm
TCRβ	H57-597	169Tm	Fluidigm
NK1.1	PK136	170Er	Fluidigm
CD44	IM7	171Yb	Fluidigm
CD4	RM4-5	172Yb	Fluidigm
B220	RA3-6B2	176Yb	Fluidigm
NKp46 (CD334)	29A1.4	167Er	Fluidigm

Ir-intercalator (1:1,000 dilution)

Rh103 (1:2,000 dilution)